Effects of an Oscillating Electric Field on and Dipole Moment Measurement of a Single Molecular Ion

Alejandra L. Collopy,[1] Julian Schmidt,[2,*] Dietrich Leibfried,[2] David R. Leibrandt,[2] and Chin-Wen Chou[2]
[1]National Institute of Standards and Technology, Boulder, Colorado 80305, USA
[2]National Institute of Standards and Technology, Boulder, Colorado 80305, USA
and Department of Physics, University of Colorado, Boulder, Colorado 80309, USA

(Received 20 July 2022; revised 29 March 2023; accepted 21 April 2023; published 31 May 2023)

We characterize and model the Stark effect due to the radio-frequency (rf) electric field experienced by a molecular ion in an rf Paul trap, a leading systematic in the uncertainty of the field-free rotational transition. The ion is deliberately displaced to sample different known rf electric fields and measure the resultant shifts in transition frequencies. With this method, we determine the permanent electric dipole moment of CaH^+, and find close agreement with theory. The characterization is performed by using a frequency comb which probes rotational transitions in the molecular ion. With improved coherence of the comb laser, a fractional statistical uncertainty for a transition line center of as low as 4.6×10^{-13} was achieved.

DOI: 10.1103/PhysRevLett.130.223201

Significant efforts are currently devoted to achieve precision spectroscopy and quantum state control of molecules. A much larger variety of molecules exists, compared to atoms, and they possess richer structures that promise entirely different functionalities and increased suitability for certain tasks, for example, greater sensitivities for various tests of fundamental physics [1–4]. High internal state coherence and the potential for conversion of quantum information across many decades in frequency also make molecules attractive for quantum information processing [5–9]. Despite impressive progress in recent years, quantum state preparation, detection, and control of molecules remains more difficult than for atoms [10–14].

Quantum-logic spectroscopy (QLS) [15] shows great promise and versatility for the study of charged particles in general and molecular ions in particular. It relies on an atomic "logic" ion species for performing sympathetic cooling of the joint translational motion and for state readout, and enables quantum-state preparation, manipulation, and spectroscopy of charged particles ("spectroscopy" ions) that are difficult to control otherwise [16–18]. All lasers addressing the molecular ion in our experiments drive far-detuned stimulated two-photon Raman transitions that do not rely on a particular level structure of a molecule. This, along with the fact that sympathetic cooling of translational degrees of freedom and quantum-logic readout can also be performed with few requirements on the details of the molecular structure, makes QLS available to a wide variety of ion species.

To explore new applications of molecules, it is also critical to measure transition frequencies and other properties with high resolution and to account for minute systematic effects that become relevant at this unprecedented level of precision. In particular, spins and the relative motion of nuclei add degrees of freedom and coupling mechanisms to the environment that are not present in atoms. For example, the ac Stark shift suffered by neutral polar molecules when trapped in optical lattices or tweezers needs to be carefully controlled to retain long coherence times [12,19,20], and understanding of trap shifts due to electric and magnetic fields are critical for high-precision molecular spectroscopy in ion traps [3,21,22]. Most molecules possess a permanent electric dipole moment, which can couple to other dipoles or external electric fields. *Ab initio* calculation of the dipole moment requires precise knowledge of the molecule's electronic structure. Measuring the dipole moment of molecular ions is challenging due to the strong Coulomb interaction with external electric fields [23,24]. Determining the dipole moment can help confirm theoretical molecular structure calculations, as well as provide information on the strength of rotational transitions driven by electric fields, or the strength of the dipole-dipole interaction that could be used to perform quantum logic gates between molecular ions [6].

In this Letter, we improve the resolution of two-photon stimulated Raman spectroscopy on the rotational states of the CaH^+ ion by an order of magnitude compared to our previous work [17], which enables precise investigation of the effects of the radio-frequency (rf) electric field in a rf trap on rotational transition frequencies. We perform spectroscopy at sub-part-per-trillion precision by driving a rotational transition at ~2 terahertz with a highly coherent frequency comb. rf electric fields at the molecular ion position can lead to coupling and level shifts of order part-per-billion that can be precisely measured. By independent *in situ* sensing of the rf electric field with the Ca^+ logic ion, we characterize the Stark shift and determine the permanent electric dipole moment of the molecular ion.

Trapped ions in rf traps can undergo micromotion [25,26]—position-dependent driven motion at the angular frequency $\Omega_{\rm rf} = 2\pi f_{\rm rf}$ of the rf drive that provides confinement of the ions. Some ion traps are specifically designed to have high symmetry to minimize the rf electric field at the trap center, but even then the time dilation shift and Stark shift due to the rf electric field need to be accurately measured and controlled for precision experiments [27]. Various methods have been developed to characterize micromotion and the electric field that drives it [25,26]. In dipolar molecular ions, the rf electric field $\vec{E}_{\rm rf}$ can interact with the permanent electric dipole moment $\vec{d}$ of the molecule via the interaction Hamiltonian

$$H = -\vec{d}\cdot\vec{E}_{\rm rf}\cos(\Omega_{\rm rf}t), \tag{1}$$

and thereby affect rotational states $|J,M\rangle$ with principal quantum number J and projection quantum number M. For linear molecules with no component of the angular momentum along the molecular axis, the perturbation in H first order in $\vec{E}_{\rm rf}$ vanishes [28,29]. The second order yields the matrix element between rotational states $|J,M\rangle$ and $|J',M'\rangle$ for the quadratic Stark effect

$$\langle J',M'|H^{(2)}|J,M\rangle = \frac{1}{4h}\sum_i \frac{\langle J',M'|\vec{d}\cdot\vec{E}_{\rm rf}|i\rangle\langle i|\vec{d}\cdot\vec{E}_{\rm rf}|J,M\rangle}{f_{\rm rf}-\nu_{J,i}} + \frac{\langle J',M'|\vec{d}\cdot\vec{E}_{\rm rf}|i\rangle\langle i|\vec{d}\cdot\vec{E}_{\rm rf}|J,M\rangle}{-f_{\rm rf}-\nu_{J,i}}, \tag{2}$$

where the sum runs over all intermediate states with nonzero matrix elements, namely, $|i\rangle = |J_i,M_i\rangle$, $0 \le J_i = J\pm 1$, $M_i = M + \{-1,0,1\}$ and $|M_i| \le J_i$. The frequency $\nu_{J,i} = (E_i - E_J)/h$ is proportional to the difference between rotational state energies E_J and E_i, and h is the Planck constant. Setting $E_{\rm rf} = |\vec{E}_{\rm rf}|$ reveals that the matrix elements are of order $C_J = d^2E_{\rm rf}^2/[4hB_R2(J+1)]$, small compared to the rotational energy $E_{\rm rot} \approx hB_RJ(J+1)$ for typical dipole moments and amplitudes of the rf electric field. For example, the rotational constant of CaH^+ is $B_R = 142.501\,7779(17)$ GHz [17] while the matrix elements are $\le h(1\ \text{kHz})$ for typical fields. Only matrix elements of nearly degenerate states with $J = J'$ are non-negligible and $f_{\rm rf}$ (~86 MHz in this Letter) can be neglected compared to $\nu_{J,i}$ in Eq. (2). Higher order rotational constants [17] can be taken into account for E_J, but will contribute below 10^{-3} relative to the lowest order proportional to B_R for the states we explored experimentally. In this approximation the matrix element for $J = 0$ is

$$H^{(2)}_{0,0} = -\frac{d^2E_{\rm rf}^2}{12hB_R}. \tag{3}$$

For fixed $J > 0$, $|M_J| \le J$ and the rf field decomposed into spherical components (see Ref. [29]) $\vec{E}_{\rm rf} = E_{\rm rf}(\epsilon_{-1}\vec{n}_{\sigma^-} + \epsilon_0\vec{n}_\pi + \epsilon_1\vec{n}_{\sigma^+})$, the nonzero matrix elements $\langle J,M'|H^{(2)}|J,M\rangle = H^{(2)}_{M,M'}$ are

$$\begin{aligned}
H^{(2)}_{M,M} &= C_J\frac{J(J+1)-3M^2}{J(2J-1)(2J+3)}[2\epsilon_0^2-(\epsilon_{-1}^2+\epsilon_1^2)],\\
H^{(2)}_{M,M+1} &= C_J\frac{3(2M+1)\sqrt{J+J^2-M(M+1)}}{\sqrt{2}J(2J-1)(2J+3)}\epsilon_0(\epsilon_1-\epsilon_{-1}),\\
H^{(2)}_{M,M+2} &= C_J\frac{3\sqrt{(J-M-1)(J-M)(J+M+1)(J+M+2)}}{J(2J-1)(2J+3)}\epsilon_{-1}\epsilon_1.
\end{aligned} \tag{4}$$

For an rf field along the quantization axis, $\epsilon_0 = 1$, $\epsilon_{-1} = \epsilon_1 = 0$, $H^{(2)}_{M,M}$ agrees with the result in [28], Chap. 10, Eq. (10.8) when setting the average square of the rf electric field equal to $E_{\rm rf}^2/2$.

We evaluate the effect of the trap rf electric field by driving transitions within and between rotational manifolds of the CaH^+ ion subjected to a variety of rf electric field configurations. That reduces the contribution of the rf electric field to the systematic uncertainty of the field-free frequency of a rotational transition by more than an order of magnitude [17]. Additionally, characterizing the effect of varying the magnitude of trap rf electric field at the molecular ion enables measurement of the molecular electric dipole moment of the CaH^+ ion for the first time. The electric dipole moment of other suitable molecular ions could be determined through the same procedure.

The steps to prepare a pure quantum state of the molecule have been described before [17]. In brief, Doppler cooling, electromagnetically induced-transparency cooling, and resolved sideband cooling of the Ca^+-CaH^+ ion crystal is performed on the Ca^+ ion. Several of the motional modes shared by both ions are cooled to the ground state, including the axial out-of-phase mode, which

is used for QLS. A series of motional sideband pulses on the molecule involving the QLS mode followed by ground state cooling on the atomic ion ("pumping cycles") [16] are used to drive the molecule from a mixture of states determined by the thermal environment towards certain target states in rotational manifolds with $1 \leq J \leq 6$ within the $^1\Sigma$ vibronic ground state. Each target state has an associated "signature transition" with a unique frequency. Sequentially driving motion-adding sidebands on the signature transitions can add a quantum of motion to the QLS mode if the molecule was in the corresponding target state. The quantum of motion can be detected by driving a motion-subtracting sideband on the Ca^+ ion and reading out its final internal state. Ideally, if the readout indicates a successful motion-subtracting transition on Ca^+, the molecule is projected into the final state of its preceding motion-adding transition. The sequence prepares the molecule in a known pure quantum state and heralds it nondestructively.

Following preparation, further spectroscopic pulses can be driven, which may change the molecular internal state. If the spectroscopic pulse changes the state of the molecule, departure from the initial state can be detected in a similar way as arrival during preparation, signaled by a negative result. Repeated cycles allow for accumulation of statistics. Stimulated Raman two-photon transitions that change J by ± 2 are driven by a Ti:sapphire frequency comb centered at $\sim$800 nm, as described in more detail in [17]. Compared to that work, the comb has been improved. Following [30], a small fraction ($\approx$40 mW) is split off the frequency comb output and spectrally broadened with a nonlinear fiber to facilitate stabilizing the repetition rate to a narrow-linewidth continuous-wave laser as an optical frequency reference [29]. The optical frequency reference improves the comb coherence, which enables longer probe times and higher spectral resolution of transitions in our setup. The unbroadened main portion of the frequency comb output, after proper power control, is used to perform rotational spectroscopy as described in [17]. Because the magnetic moment of the hydrogen nucleus and the rotational magnetic moment couple together, energy eigenstates of CaH^+ are superpositions of the product states $|J, M\rangle|\frac{1}{2}, \pm\frac{1}{2}\rangle$, where the second ket represents the magnitude and projection of the proton spin on the quantization axis. We use the notation $|J, m, \xi\rangle$ [16,17], where $m = M \pm 1/2$ denotes the joint projection of rotational angular momentum and proton spin along the quantization axis, which remains a good quantum number and $\xi = \{+, -\}$ labels one of the two eigenstates that share the same J and m, except for $|J, m = \pm(J + 1/2), \pm\rangle = |J, \pm J\rangle|1/2, \pm 1/2\rangle$. After preparing the molecule in $|2, -5/2, -\rangle$, a 128 ms square envelope pulse train of the Raman beams derived from the frequency comb is applied to the molecular ion, followed by an attempt to detect the initial molecular state. Figure 1 depicts the result

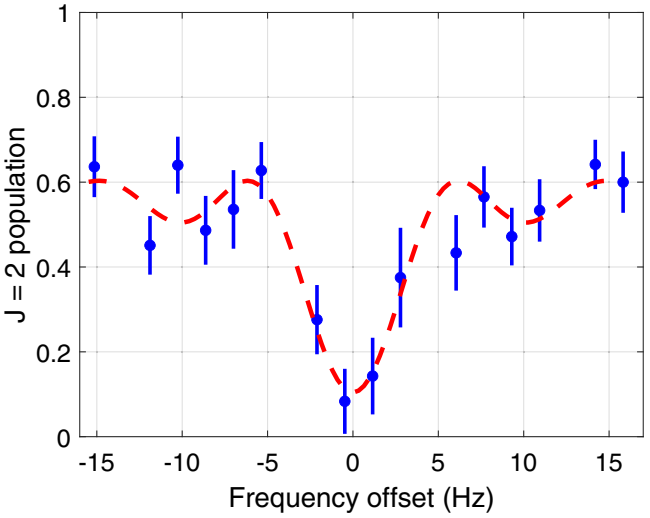

FIG. 1. Population in the initial $|J = 2, m = -5/2, -\rangle$ rotational state vs the Raman difference frequency offset to the center of the line model (dashed red line) of the $|2, -5/2, -\rangle \rightarrow |4, -7/2, -\rangle$ rotational transition at approximately 2 THz. Error bars indicate a 68% confidence interval. The number of probes ranges for each data point from 10 to 65 and was given by the probabilistic preparation of the initial state of the molecule. Dashed line shows the least squares fit of a Rabi line shape with free parameters of center frequency offset, remaining population, contrast, and Rabi rate, with pulse duration fixed. The fit yields a 0.9 Hz statistical uncertainty (95% confidence). The 128 ms probe time is a substantial fraction of the observed lifetime of the initial state, resulting in reduced contrast of the line.

of scanning the frequency difference between the Raman beams over the resonance of the transition to $|J' = 4, -7/2, -\rangle$ at $\sim$2 THz (line $Q \approx 3.3 \times 10^{11}$). A fit to a Rabi line shape for a square spectroscopy pulse [31] yields a statistical uncertainty of the line center of $\sim$0.9 Hz, corresponding to a fractional statistical uncertainty of 4.6×10^{-13}. This compares favorably with the resolution of rotational spectroscopy on molecular ions in other experiments [21,22].

To characterize the effect of the rf electric field on rotational transitions in the molecular ion, we vary and measure the direction and amplitude of the field at the molecular ion. As schematically shown in Fig. 2, we utilize nearby electrodes to manipulate the position of the ions and thereby the rf electric field amplitude and direction experienced by the molecular ion. Imperfections of the electrode geometry of the trap used in our experiments results in a nonzero minimal rf-field amplitude of approximately 1 kV/m. We can characterize the rf electric field by exchanging the positions of the atom and the molecule and using the atom to probe the rf-electric field amplitude and direction by measuring the micromotion sideband-to-carrier Rabi-rate ratios of the narrow 729 nm quadrupole transition [26] (also see Supplemental Material [29]). Three 729 nm laser beams are directed along the magnetic

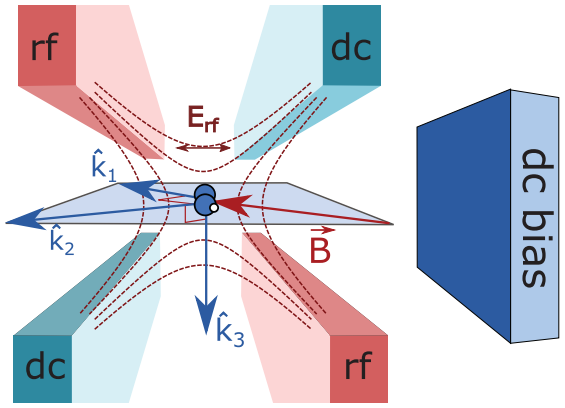

FIG. 2. An ideal linear rf trap forms an electric quadrupole field with a null along the trap axis. Ions positioned off of the null experience a rf electric field. Because of the electrode geometry of the trap used in our experiments, the rf-electric field along the ion-ion axis has a finite minimal amplitude. By adjusting the voltages applied to the dc electrodes and the more distant dc bias electrode, the ions can be intentionally shifted from this minimum to sample different rf electric field magnitudes and directions. Three 729 nm laser beams are used to measure micromotion along approximately mutually orthogonal directions, $\hat{k}_1$ parallel to the magnetic quantization axis $\vec{B}$, $\hat{k}_2$, and $\hat{k}_3$.

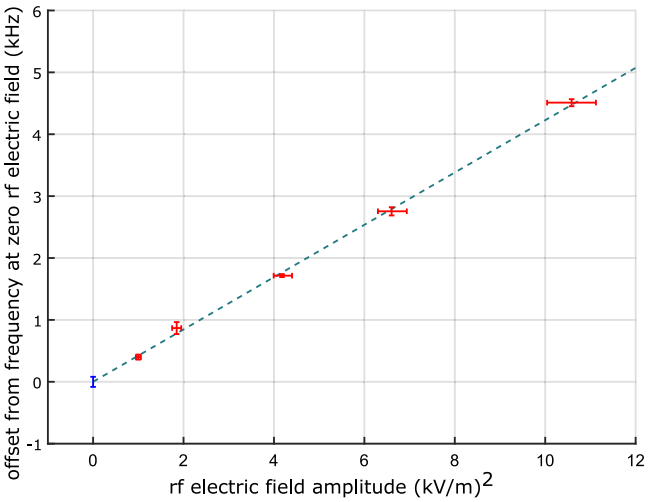

FIG. 3. Red markers show the measured shifts in frequencies of the $|2,-3/2,-\rangle$ to $|0,-1/2,-\rangle$ transition as a function of the squared rf electric field amplitude at the molecular ion location. Spectroscopic probe times varied from 2.5 to 20.5 ms for different data points. The blue marker shows the rf electric field-free transition frequency (95% confidence interval $[-82, 80]$ Hz) obtained through extrapolation to zero field with uncertainties determined by parametric bootstrapping. The dashed green line is a linear fit to the data. Its slope can be used to determine the permanent dipole moment of the ion.

quantization axis as well as two directions orthogonal to that axis and each other, respectively. The experimentally determined Rabi-rate ratios can, with some assumptions, be inverted to yield three orthogonal components of the rf electric field amplitude [29].

Rotational states of CaH^+ with the same J can have energy splittings smaller than 1 kHz in the approximately 0.36 mT static magnetic field in our experiment. The rf electric field can cause significant mixing of near-degenerate electric field-free eigenstates of the molecule [16] and modeling of transitions becomes quite involved [29]. A relatively simple case where spin, rotation, and electric field decouple arises for the extreme $|J,\pm(J+1/2),\pm\rangle$ states when rf electric field and static magnetic field are parallel [29], but technical constraints in our setup prevent changing the rf electric field magnitude in this arrangement. Because the $J=0$ rotational level is the most sensitive to the rf electric field, we measure the frequency of the ~855 GHz transition $|2,-3/2,-\rangle$ to $|0,-1/2,-\rangle$ as a function of the electric field amplitude due to the rf drive, as shown in Fig. 3. Vertical error bars represent the 95% confidence interval of the line center when fitting transition line shapes similar to the one shown in Fig. 1, while horizontal errors are set by uncertainty in determining the electric field at the position of the molecule [29]. Fitting of the slope and intercept is performed by parametric bootstrapping [29]. The rf electric field-free transition frequency can be found from the intercept of this fit with a 95% confidence interval of [-82, 80] Hz. This uncertainty is more than 1 order of magnitude smaller than that in the previous measurements [17].

The dependence of the rotational transition frequency on the rf electric field can be used to determine the electric dipole moment of the molecule. In particular, we can bound the shift of the initial state $|2,-3/2,-\rangle$, which has a particularly small dependence on the rf electric field, by modeling the effect of the field on the eigenstates of the molecule and their energies [29]. We find that $|2,-3/2,-\rangle$ shifts by no more than 50 Hz for any of the rf amplitudes used in the experiments and account for this by adding 50 Hz in quadrature to the frequency uncertainties shown in Fig. 3. In this approximation, the frequency shifts can be attributed to the state $|0,-1/2,-\rangle$, described by Eq. (3), and only depend on the amplitude of the rf electric field experienced by the molecule. The slope of the fit function shown in Fig. 3 yields a value of $d = 17.81 \pm 0.63 \times 10^{-30}$ C m (5.34 ± 0.19 Debye) for the permanent electric dipole moment of CaH^+, with the 95% confidence interval found by parametric bootstrapping, in agreement with the theoretical value of 5.310 Debye [35]. To the best of our knowledge, this is the first experimental determination of the permanent dipole moment of a molecular ion using this method.

In future work, we can improve the uncertainty of field-free transition frequency measurements due to the rf electric field by using a more symmetric trap with smaller minimal rf electric field amplitude at the position of the

molecule. Uncertainties in determining micromotion could be improved by better control of the 729 nm beam directions, or by using different methods [26]. State preparation can be more efficient by using the frequency comb and/or a microwave source addressing the $J'' = 0$ to $J' = 1$ transition to prepare molecules in a target rotational state. Our approach is suitable for molecular spectroscopy and electric dipole measurements on a variety of other molecular species, given that the molecule of interest is not too disparate in charge-to-mass ratio from that of the logic ion. We demonstrate versatile control techniques based on QLS that are stepping stones towards interrogating increasingly complex molecules, such as polyatomics, with the potential to distinguish isotopomers, isomers, and possibly even the chirality of molecular ions, which may be particularly advantageous for tests of fundamental physics [36,37].

In conclusion, we characterize the Stark effect due to the rf electric field experienced by the molecular ion and account for its effect on the measured transition frequencies, improving the systematic uncertainty of a rf electric field-free rotational transition frequency in the molecular ion by an order of magnitude from our previous work [17]. In addition, we determine the electric dipole moment of the CaH^+ molecular ion, illustrating the use of the rf field in an ion trap for measuring a molecular property. We demonstrate sub-part-per-trillion resolution rotational spectroscopy of CaH^+ using methods that are suitable for a wide range of molecular ion species, including some of interest for tests of fundamental physics.

We thank D. Hume for alerting us to the potential effects of the rf trap drive on transition frequencies, T. Fortier and S. Diddams for their advice on improving the frequency comb coherence, and L. Sinclair and Y. Liu for careful reading and their suggestions on the manuscript. This work was partially supported by the U.S. Army Research Office (Grant No. W911NF-19-1-0172). During this work A. L. C. was supported by a National Research Council postdoctoral fellowship. J. S. gratefully acknowledges support from the Alexander von Humboldt Foundation.

*Present address: Paul Scherrer Institute, Forschungsstrasse 111, 5232 Villigen PSI, Switzerland.

[1] M. Kajita, G. Gopakumar, M. Abe, M. Hada, and M. Keller, Phys. Rev. A **89**, 032509 (2014).
[2] V. Andreev, D. G. Ang, D. DeMille, J. M. Doyle, G. Gabrielse, J. Haefner, N. R. Hutzler, Z. Lasner, C. Meisenhelder, B. R. O'Leary, C. D. Panda, A. D. West, E. P. West, and X. Wu, Nature (London) **562**, 355 (2018).
[3] W. B. Cairncross, D. N. Gresh, M. Grau, K. C. Cossel, T. S. Roussy, Y. Ni, Y. Zhou, J. Ye, and E. A. Cornell, Phys. Rev. Lett. **119**, 153001 (2017).
[4] O. Grasdijk, O. Timgren, J. Kastelic, T. Wright, S. Lamoreaux, D. DeMille, K. Wenz, M. Aitken, T. Zelevinsky, T. Winick, and D. Kawall, Quantum Sci. Technol. **6**, 044007 (2021).
[5] D. DeMille, Phys. Rev. Lett. **88**, 067901 (2002).
[6] E. R. Hudson and W. C. Campbell, Phys. Rev. A **98**, 040302 (R) (2018).
[7] V. V. Albert, J. P. Covey, and J. Preskill, Phys. Rev. X **10**, 031050 (2020).
[8] K. Najafian, Z. Meir, and S. Willitsch, Phys. Chem. Chem. Phys. **22**, 23083 (2020).
[9] Y. Lin, D. R. Leibrandt, D. Leibfried, and C.-W. Chou, Nature (London) **581**, 273 (2020).
[10] F. Wolf, Y. Wan, J. C. Heip, F. Gebert, C. Shi, and P. O. Schmidt, Nature (London) **530**, 457 (2016).
[11] M. Sinhal, Z. Meir, K. Najafian, G. Hegi, and S. Willitsch, Science **367**, 1213 (2020).
[12] S. Burchesky, L. Anderegg, Y. Bao, S. S. Yu, E. Chae, W. Ketterle, K. K. Ni, and J. M. Doyle, Phys. Rev. Lett. **127**, 123202 (2021).
[13] M. Fan, C. A. Holliman, X. Shi, H. Zhang, M. W. Straus, X. Li, S. W. Buechele, and A. M. Jayich, Phys. Rev. Lett. **126**, 023002 (2021).
[14] J. R. Li, W. G. Tobias, K. Matsuda, C. Miller, G. Valtolina, L. De Marco, R. R. Wang, L. Lassablière, G. Quéméner, J. L. Bohn, and J. Ye, Nat. Phys. **17**, 1144 (2021).
[15] P. O. Schmidt, T. Rosenband, C. Langer, W. M. Itano, J. C. Bergquist, and D. J. Wineland, Science **309**, 749 (2005).
[16] C.-W. Chou, C. Kurz, D. B. Hume, P. N. Plessow, D. R. Leibrandt, and D. Leibfried, Nature (London) **545**, 203 (2017).
[17] C.-W. Chou, A. L. Collopy, C. Kurz, Y. Lin, M. E. Harding, P. N. Plessow, T. Fortier, S. Diddams, D. Leibfried, and D. R. Leibrandt, Science **367**, 1458 (2020).
[18] P. Micke, T. Leopold, S. A. King, E. Benkler, L. J. Spieß, L. Schmöger, M. Schwarz, J. R. Crespo López-Urrutia, and P. O. Schmidt, Nature (London) **578**, 60 (2020).
[19] S. Kotochigova and D. DeMille, Phys. Rev. A **82**, 063421 (2010).
[20] P. D. Gregory, J. A. Blackmore, S. L. Bromley, and S. L. Cornish, Nat. Phys. **17**, 1149 (2021).
[21] S. Alighanbari, G. S. Giri, F. L. Constantin, V. I. Korobov, and S. Schiller, Nature (London) **581**, 152 (2020).
[22] S. Patra, M. Germann, J. P. Karr, M. Haidar, L. Hilico, V. I. Korobov, F. M. Cozijn, K. S. Eikema, W. Ubachs, and J. C. Koelemeij, Science **369**, 1238 (2020).
[23] J. K. Thompson, S. Rainville, and D. E. Pritchard, Nature (London) **430**, 58 (2004).
[24] H. Loh, Search for an electron electric dipole moment with trapped molecular ions, Ph.D. thesis, University of Colorado, Boulder, 2013.
[25] D. J. Berkeland, J. D. Miller, J. C. Bergquist, W. M. Itano, and D. J. Wineland, J. Appl. Phys. **83**, 5025 (1998).
[26] J. Keller, H. L. Partner, T. Burgermeister, and T. E. Mehlstäubler, J. Appl. Phys. **118**, 104501 (2015).
[27] S. M. Brewer, J. S. Chen, A. M. Hankin, E. R. Clements, C.-W. Chou, D. J. Wineland, D. B. Hume, and D. R. Leibrandt, Phys. Rev. Lett. **123**, 033201 (2019).
[28] C. H. Townes and A. L. Schawlow, *Microwave Spectroscopy* (Dover, Mineola, NY, 1975).
[29] See Supplemental Material at http://link.aps.org/supplemental/10.1103/PhysRevLett.130.223201 for additional information on methods, which includes Refs. [16,26,30–34].

[30] A. Bartels, S. A. Diddams, T. M. Ramond, and L. Hollberg, Opt. Lett. **28**, 663 (2003).
[31] D. J. Wineland, C. Monroe, W. M. Itano, D. Leibfried, B. E. King, and D. M. Meekhof, J. Res. Natl. Inst. Stand. Technol. **103**, 259 (1998).
[32] W. H. Press, S. A. Teukolsky, W. T. Vetterling, and B. P. Flannery, Modeling of data, in *Numerical Recipes in C The Art of Scientific Computing* (Press Syndicate of the University of Cambridge, New York, NY, 1992), pp. 656–706.
[33] C. Kurz, Quantum networking with single ions and single photons interfaced in free space, Ph.D. thesis, Saarbrcken Germany, 2015.
[34] H. C. J. Gan, G. Maslennikov, K.-W. Tseng, T. R. Tan, R. Kaewuam, K. J. Arnold, D. Matsukevich, and M. D. Barrett, Phys. Rev. A **98**, 032514 (2018).
[35] M. Abe, M. Kajita, M. Hada, and Y. Moriwaki, J. Phys. B **43**, 245102 (2010).
[36] D. Patterson, Phys. Rev. A **97**, 033403 (2018).
[37] N. R. Hutzler, Quantum Sci. Technol. **5**, 044011 (2020).